Journal of Metals, Materials and Minerals, 35(4), e2448, 2025

Synthesis and characterization of silica nanoparticles from solar panel glass cullet

Pathomporn USSAWANAWACHAT[1], Nithiwach NAWAUKKARATHARNANT[1,2], and Apirat THEERAPAPVISETPONG[1,*]

[1] *Upcycled Materials from Industrial and Agricultural Wastes Research Unit, Department of Materials Science, Faculty of Science, Chulalongkorn University, Bangkok, 10330, Thailand*

[2] *Metallurgy and Materials Science Research Institute, Chulalongkorn University, Bangkok, 10330, Thailand*

***Corresponding author e-mail**: Apirat.t@chula.ac.th

Received date:
27 June 2025
Revised date:
1 September 2025
Accepted date:
23 September 2025

Keywords:
Silica nanoparticles;
Solar panel recycling;
Alkali fusion;
Glass cullet;
Polyethylene glycol

Abstract

The rapid growth of solar energy as a renewable resource has led to a significant increase in discarded solar panels. Recycling their glass components, especially fine cullet fragments, remains a major challenge due to impurity levels and processing limitations. This study proposes a sustainable approach to recycle solar panel glass cullet into high-purity silica nanoparticles using alkali fusion followed by acid precipitation. Process conditions including cullet to NaOH ratio, fusion temperature, and surfactant addition were optimized. The highest silica yield of 60.26% was achieved at a 1:1.4 cullet to NaOH ratio and 500°C. Polyethylene glycol (PEG 1000) was used as a surfactant to reduce agglomeration and enhancing surface characteristics. BET analysis showed that PEG addition increased the specific surface area to 372.34 $m^2 \cdot g^{-1}$ and formed a compact mesoporous structure with an average pore size of 8.91 nm. In comparison, samples without PEG exhibited a larger pore size of 12.36 nm and a lower surface area of 360.24 $m^2 \cdot g^{-1}$. EDX confirmed the high purity of the synthesized silica, with 95.12% SiO_2. These findings demonstrate a practical and environmentally beneficial method to convert problematic solar panel waste into valuable nanomaterials, supporting sustainable resource recovery and circular economy goals.

1. Introduction

The global energy landscape has undergone a significant transformation in the past decade, with a pronounced shift toward renewable energy sources. In particular, solar power has experienced remarkable growth due to declining costs, technological improvements, and supportive policies aimed at reducing carbon emissions [1,2]. According to the International Energy Agency (IEA), solar photovoltaic (PV) capacity has shown consistent expansion over the past decade, highlighting the accelerating transition toward sustainable energy systems [3].

This rapid deployment of solar technology, while beneficial for climate goals, presents an emerging waste management challenge. The average lifespan of solar panels ranges from 25-30 years [4], creating a delayed but inevitable waste stream. Early solar panel installations from the 2000s are now approaching end-of-life, and the volume of decommissioned panels is expected to increase dramatically. By 2050, cumulative solar panel waste could reach 78 million tons globally [5].

Current recycling processes for solar panels face significant technical and economic challenges, particularly when handling glass cullet waste, which constitutes approximately 70% to 75% of a typical crystalline silicon solar panel by weight [6]. While larger glass fragments can be recovered through conventional recycling methods, smaller fragments present substantial difficulties for recycling facilities. These small-sized cullets cause maintenance issues in recycling plants due to their abrasive nature, accelerating equipment wear and increasing facility downtime [7]. Additionally, the high surface area to volume ratio of fine glass particles enhances their propensity for contamination with encapsulant materials, metals, and semiconductor residues, compromising the quality of recycled products [8,9]. Conventional mechanical separation techniques become progressively inefficient as particle size decreases, failing to achieve required purity levels for high-value glass recycling applications [10]. Furthermore, the economic viability of processing small-sized cullet is questionable, as additional processing steps increase recycling costs by an estimated factor of 2 to 3 compared to larger fragments [11], while the resulting market value often remains insufficient to offset these expenses [12].

Alternative valorization routes for glass cullet have been extensively explored in ceramic applications, demonstrating the potential for waste glass utilization in construction materials. Research has shown that soda-lime glass powder can effectively serve as a fluxing agent in ceramic bodies, reducing firing temperatures and improving mechanical properties [13]. Studies on incorporating waste glass into clay-based ceramics have demonstrated enhanced densification processes and improved technological properties when glass content is optimized [14]. The addition of soda-lime glass at 10% to 20% by weight in ceramic formulations has been shown to increase flexural strength significantly while reducing porosity and water absorption [15]. Furthermore, waste glass incorporation in ceramic systems can modify the equilibrium between glassy and crystalline phases, leading to formation of beneficial secondary phases such as anorthite and

affecting mullite formation kinetics [16,17]. While these ceramic applications demonstrate the versatility of conventional soda-lime glass cullet, solar panel glass offers distinct advantages due to its superior purity profile. Solar panel glass typically contains higher silica content and lower levels of impurities compared to conventional soda-lime glass, making it particularly suitable for high-value applications such as silica nanoparticles synthesis where purity is critical for achieving desired material properties and performance [18].

Converting waste glass cullet into silica nanoparticles offers a promising upcycling pathway with significant applications across industries. Silica nanoparticles derived from waste glass exhibit high specific surface area, enhanced reactivity, and excellent mechanical properties [19]. In construction, it serves as a supplementary cementitious material that increases concrete strength by 15% to 25% while reducing cement consumption and carbon emissions [20,21]. In polymers, it functions as a reinforcing filler enhancing mechanical and thermal properties [22]. Additional applications include catalyst supports [23] and environmental remediation where silica nanoparticles demonstrate superior pollutant adsorption [24]. The transformation of low-value glass cullet into high-value silica nanoparticles creates potential circular economy opportunities that address waste management challenges while adding significant economic value [25,26].

Previous studies have explored the conversion of waste glass into silica nanoparticles using various synthesis approaches. For instance, waste soda-lime glass has been utilized as a precursor through alkali fusion with NaOH [27], which reacts with silica to form soluble sodium silicate, followed by acid precipitation to recover silica nanoparticles. Other works employed sol–gel routes or hydrothermal methods, often with the addition of surfactants such as polyethylene glycol (PEG) to control particle agglomeration [28,29]. These studies demonstrated the feasibility of valorizing waste glass into silica nanoparticles; however, limitations remain in terms of silica yield, product purity, and control over particle morphology. In particular, silica nanoparticles synthesized from general waste glass powders often exhibited relatively low surface areas and moderate purity levels, restricting their potential for high-value applications.

This research utilized a two-step method involving alkali fusion followed by acid precipitation to synthesize silica nanoparticles from solar panel glass cullet. The study examined the effect of process parameters such as chemical ratios, thermal treatment, and solution conditions on silica dissolution, yield, and particle size. Unlike earlier studies that used conventional waste glass and often reported moderate yield, low purity, and limited particle control, this work applied solar panel cullet and systematically optimized the synthesis route, including PEG assisted precipitation. Overall, this work demonstrates a sustainable pathway for converting photovoltaic waste into high value silica nanoparticles, offering both environmental benefits and potential for advanced material applications.

2. Experimental and details

2.1 Materials

Solar panel glass cullet was obtained from decommissioned solar panels. Analytical grade sodium hydroxide (NaOH, 99%, Krungthep-chemi) was used for the alkali fusion process. Hydrochloric acid (HCl, 37%, Qrec) was utilized for the acid precipitation process. Polyethylene glycol (PEG 1000, Sigma-Aldrich) was used as a surfactant, and ethyl alcohol (99.9%, Qrec) was used as co-solvent to control particle size and reduce agglomeration. All other chemicals used were of analytical grade and used without further purification. Deionized water was used throughout the experiments.

2.2 Preparation of solar panel glass cullet

The preparation of solar panel glass cullet followed a multi-step process to obtain fine powder suitable for the alkali fusion reaction. First, the solar panel glass cullet was reduced in size using a vibratory disc mill. The crushed material was then subjected to wet milling in a high-speed ball mill for 30 min, using a 1:1 cullet to water weight ratio. The resulting slurry was sieved through a 325-mesh (45 μm) screen to obtain fine particles. The fine powder was then dried at 110°C for 24 h to remove moisture and stored in a desiccator until further use.

2.3 Synthesis of silica nanoparticles

2.3.1 Alkali fusion

The alkali fusion process was conducted by mixing the fine solar panel glass cullet powder with NaOH at three different weight ratios: 1:1, 1:1.2, and 1:1.4 (cullet:NaOH). Each mixture was then heated in furnace at three different temperatures 500°C, 600°C, and 700°C for 3 h with a heating rate of 5°C·min^{-1}. The water soluble sodium silicate phase was produced as in Equation (1) [30].

$$SiO_2 + 2NaOH \rightarrow Na_2SiO_3 + H_2O \quad (1)$$

After fusion, the samples were allowed to cool to room temperature and were then ground to obtain a fine powder.

2.3.2 Preparation of sodium silicate solution

5 g of the fused material was dissolved in varying volumes of deionized water 20 mL, 40 mL, and 60 mL to assess the effect of water volume on the dissolution process. The mixtures were stirred for 1 h at room temperature. The resulting slurries were vacuum filtered to separate the undissolved residue from the sodium silicate solution. The undissolved residue was dried at 110°C for 24 h and weighed to calculate the dissolution efficiency. The volume and pH of the resulting sodium silicate solutions were recorded.

2.3.3 Acid precipitation

The sodium silicate solutions were subjected to acid precipitation to obtain silica nanoparticles. The pH of each solution was adjusted to 5 using 2M HCl, which caused the precipitation of silica gel according to the following reaction on Equation (2) [30].

$$Na_2SiO_3 + 2HCl \rightarrow SiO_2 + 2NaCl + H_2O \quad (2)$$

The silica gel was collected by vacuum filtration and washed repeatedly with deionized water, ensuring the removal of sodium chloride (NaCl) and other impurities. The washed silica gel was dried at 110°C for 24 hours to obtain the final silica nanoparticles powder.

Ethanol (5 vol%) and PEG 1000 (2.5 wt%) were added to the solutions as co-solvent and surfactant, respectively. To investigate the effects of ethanol as co-solvent and PEG 1000 as surfactant on particle size and agglomeration, ethanol (5 vol%) or PEG 1000 (2.5 wt%) were added to the solutions. Additional experiments were conducted with and without these additives, focusing on the samples prepared at 500°Cwith a 1:1.4 cullet to NaOH ratio, which showed the highest yield in preliminary tests.

2.4 Characterization

The elemental composition of the original solar panel glass cullet, expressed in terms of their oxides, was determined by X-ray fluorescence (XRF) using a Rigaku ZSX Primus III+. Crystalline phases formed during the alkali fusion process were identified by X-ray diffraction (XRD, Bruker D8 Discover) operated with Cu Kα radiation (λ = 1.5418 Å) over a 2θ range of 10° to 80°. The morphology and particle size of the synthesized silica nanoparticles were examined by Scanning electron microscopy (SEM, Hitachi SU3500), with samples gold-coated to enhance conductivity. Elemental analysis of the final product was performed using energy-dispersive X-ray spectroscopy (EDX, Horiba X-maxN), providing quantitative data on silicon, oxygen, and potential impurities. Functional groups and the chemical structure of the synthesized silica were confirmed by Fourier transform infrared spectroscopy (FTIR, ThermoFisher Scientific iN10, iZ10), conducted via the ATR method in the 4000 cm^{-1} to 400 cm^{-1} range. The specific surface area, total pore volume, and average pore diameter of the silica nanoparticles were determined using the Brunauer–Emmett–Teller (BET) method, with nitrogen gas adsorption at 77 K performed on a Micromeritics 3Flex Surface Characterization Analyzer.

2.5 Yield calculation

The yield of silica nanoparticles was calculated using the following Equation (3):

$$\text{Yield (\%)} = \frac{\text{Weight of silica nanoparticles}}{\text{Weight of glass cullet x 0.6876}} \times 100 \qquad (3)$$

Where the weight of SiO_2 in the original glass cullet was determined from the XRF analysis (68.76% of the initial cullet weight).

3. Results and discussion

3.1 Characterization of solar panel glass cullet

The composition of the solar panel glass cullet was determined using XRF analysis, and the results are presented in Table 1. Silicon dioxide (SiO_2) was found to be the major component, constituting 68.76% of the cullet by mass. Other significant components included sodium oxide (Na_2O, 12.72%), calcium oxide (CaO, 10.96%), and magnesium oxide (MgO, 4.45%).

3.2 Alkali fusion and dissolution efficiency

The alkali fusion process was employed to convert the silica present in the glass cullet into soluble sodium silicate. XRD analysis of the fused powders (Figure 1) confirmed that sodium silicate was the predominant crystalline phase in all samples, regardless of the fusion temperature or the cullet to NaOH ratio. Additional crystalline phases, including sodium aluminosilicate and gehlenite, were also detected These phases formed due to the reaction of NaOH with impurities such as aluminum, calcium, and magnesium in the glass cullet. Among these, sodium aluminosilicate was soluble in strong alkaline solutions [31], while gehlenite remained largely undissolved [32], contributing to the solid residue and reducing the overall silica yield.

The efficiency of the alkali fusion process was evaluated by measuring the residue percentage after dissolution. Figure 2 presents the residue percentages for different cullet to NaOH ratios, fusion temperatures, and water volumes used during dissolution. The results indicate that increasing the NaOH ratio led to decreased residue percentages, suggesting improved dissolution efficiency. This trend can be attributed to the more complete conversion of silica into soluble sodium silicate at higher NaOH concentrations. At a 1:1.4 cullet to NaOH ratio, the residue percentage was consistently lower across all fusion temperatures and water volumes, with values generally below 20%.

3.3 Silica nanoparticles yield

The yield of silica nanoparticles was calculated based on the initial silica content in the glass cullet. Figure 3-5 present the relationship between the yield and residue percentages for different water volumes used during dissolution 20 mL, 40 mL, and 60 mL respectively. A consistent inverse relationship was observed between the residue percentage and the silica yield, lower residue percentages corresponded to higher yields, indicating that more efficient dissolution of the fused material led to improved silica recovery. The highest yield, 60.26%, was obtained using a 1:1.4 cullet to NaOH ratio at 500°C. This yield is limited by the presence of impurities in the glass cullet, which contribute to the formation of undissolved phases such as gehlenite. These phases incorporate silica into insoluble compounds, thereby reducing the amount of silica recovered. Nonetheless, the selected conditions appear to offer an optimal balance for converting silica into soluble sodium silicate while minimizing the formation of insoluble byproducts. Among the different water volumes, the 20 mL condition consistently produced the highest silica yield. This was particularly evident at the optimized 1:1.4 cullet to NaOH ratio and 500°C, where the maximum yield of 60.26% was achieved. In contrast, the yields obtained at 40 mL and 60 mL were significantly lower, as illustrated in Figure 4-5. The decline in yield with increasing water volume reflects the dilution effect, which decreases the supersaturation of sodium silicate and reduces precipitation efficiency. This optimized yield is slightly higher than the 50% commonly reported for silica nanoparticles synthesized from waste glass powders [33], suggesting that the present conditions improved dissolution and recovery while maintaining process simplicity. It should be noted that the sum of % yield and % residue does not necessarily equal 100%. The residue represents only the insoluble fraction after dissolution, while a portion of the dissolved material does not precipitate as silica during the acid precipitation step. Therefore, % residue and % yield should be considered complementary indicators of silica recovery rather than strictly additive quantities.

Table 1. Chemical composition of the solar panel glass cullet determined XRF.

Oxide	Mass [%]	Oxide	Mass [%]
SiO_2	68.76	TiO_2	0.03
Na_2O	12.72	Fe_2O_3	0.13
CaO	10.96	NiO	0.01
MgO	4.45	CuO	0.01
Al_2O_3	1.46	ZnO	0.01
SO_3	1.06	SrO	0.01
K_2O	0.06	ZrO_2	0.01
Cl	0.03	SnO_2	0.02
P_2O_5	0.01	Sb_2O_3	0.24

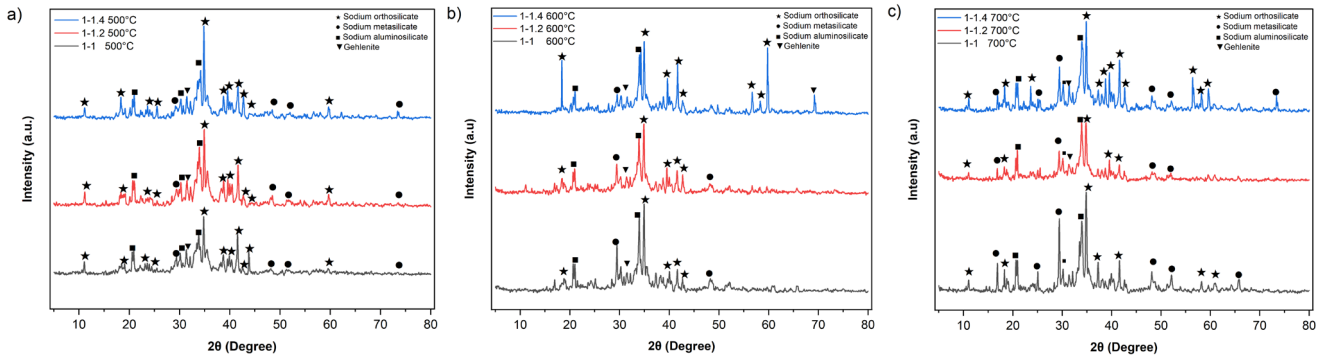

Figure 1. XRD patterns of fused powder under different chemical ratio heated at 500°C (a), 600°C (b), and 700°C (c).

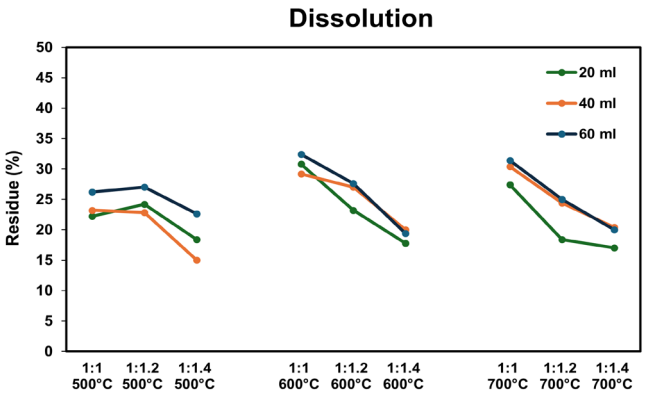

Figure 2. Residue percentage after dissolution of fused powder under different conditions.

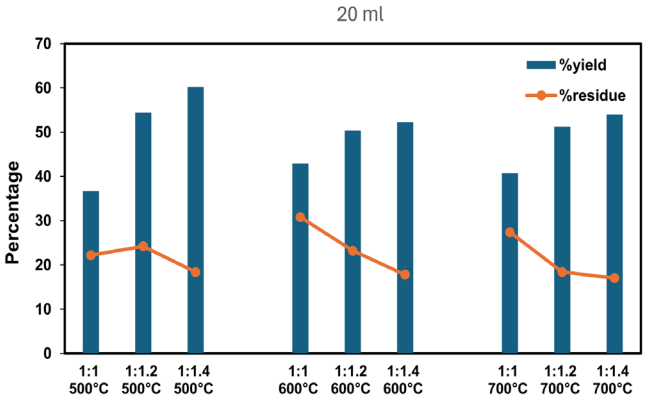

Figure 3. Percentage of yield and residue at 20 mL water volume (water volume used for dissolving 5 g of fused material during sodium silicate solution preparation).

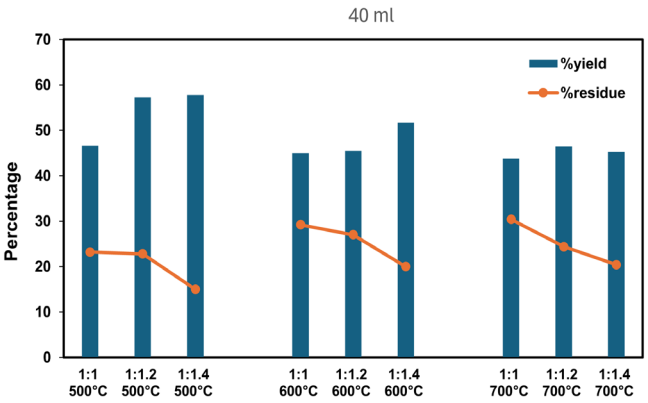

Figure 4. Percentage of yield and residue at 40 mL water volume (water volume used for dissolving 5 g of fused material during sodium silicate solution preparation).

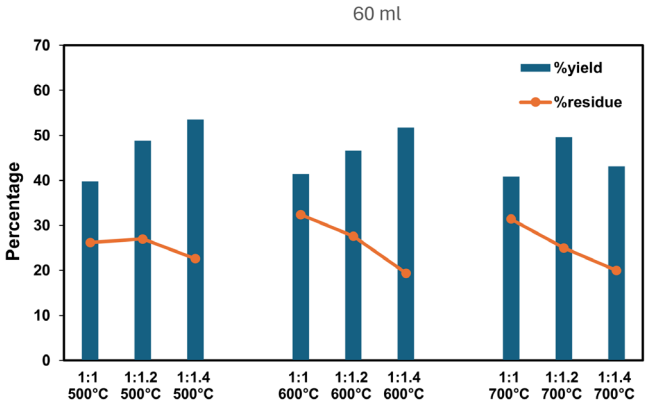

Figure 5. Percentage of yield and residue at 60 mL water volume (water volume used for dissolving 5 g of fused material during sodium silicate solution preparation).

3.4 Morphological and elemental analysis

The morphology and particle size of the synthesized silica nanoparticles were examined using SEM. Figure 6 shows SEM images of samples prepared with a 1:1.4 cullet to NaOH ratio under different fusion temperatures 500°C, 600°C, and 700°C and water volumes 20 mL, 40 mL, and 60 mL. The SEM images reveal that the water volume used during dissolution had a significant impact on particle size. This behavior can be explained by nucleation and growth kinetics. At lower water volumes (20 mL), the higher sodium silicate concentration produces rapid supersaturation, favoring numerous nucleation events and leading to smaller particles. At higher volumes (40 mL to 60 mL), the solution becomes more diluted, reducing supersaturation and nucleation frequency. Consequently, fewer nuclei are formed, but each has more time and available silicate species to grow, resulting in larger particles with smoother surfaces, as observed in SEM images. This observation is consistent across all fusion temperatures. Regarding the effect of fusion temperature, SEM images suggest that temperature did not significantly alter the final particle size distribution compared to the influence of water volume. This is likely because fusion temperature mainly affects the efficiency of sodium silicate formation rather than the nucleation–growth dynamics during precipitation. Thus, particle size was controlled primarily by the solution concentration and precipitation conditions rather than the fusion temperature.

EDX was used to analyze the elemental composition of silica nanoparticles synthesized from cullet to NaOH 1:1.4 weight ratio and fused at 500°C. The analysis (Figure 7) revealed that the silica content (SiO_2) was approximately 95.12%, calculated from 44.39 wt% Si and 54.01 wt% O. Minor impurities, including Na, Al, and Cl, were collectively below 5 wt%, indicating the high purity of the synthesized silica nanoparticles. The high silica content achieved through this synthesis route demonstrates the effectiveness of the alkali fusion and acid precipitation method for recovering high-purity silica from solar panel glass cullet. The presence of trace amounts of Na and Cl can be attributed to residual sodium chloride formed during the acid precipitation step, which could potentially be reduced through more thorough washing. The aluminum impurity likely originates from sodium aluminosilicate, a phase that is soluble in strong alkaline solutions and may remain in the sodium silicate solution after vacuum filtration. Comparable purities have also been reported in previous studies, such as 98.5% for colloidal silica nanoparticles derived from waste glass powder [33] and >92% for silica gel synthesized from waste glass bottles [27], supporting that the 95% purity obtained in this work is within the high-purity range for silica recovered from waste glass.

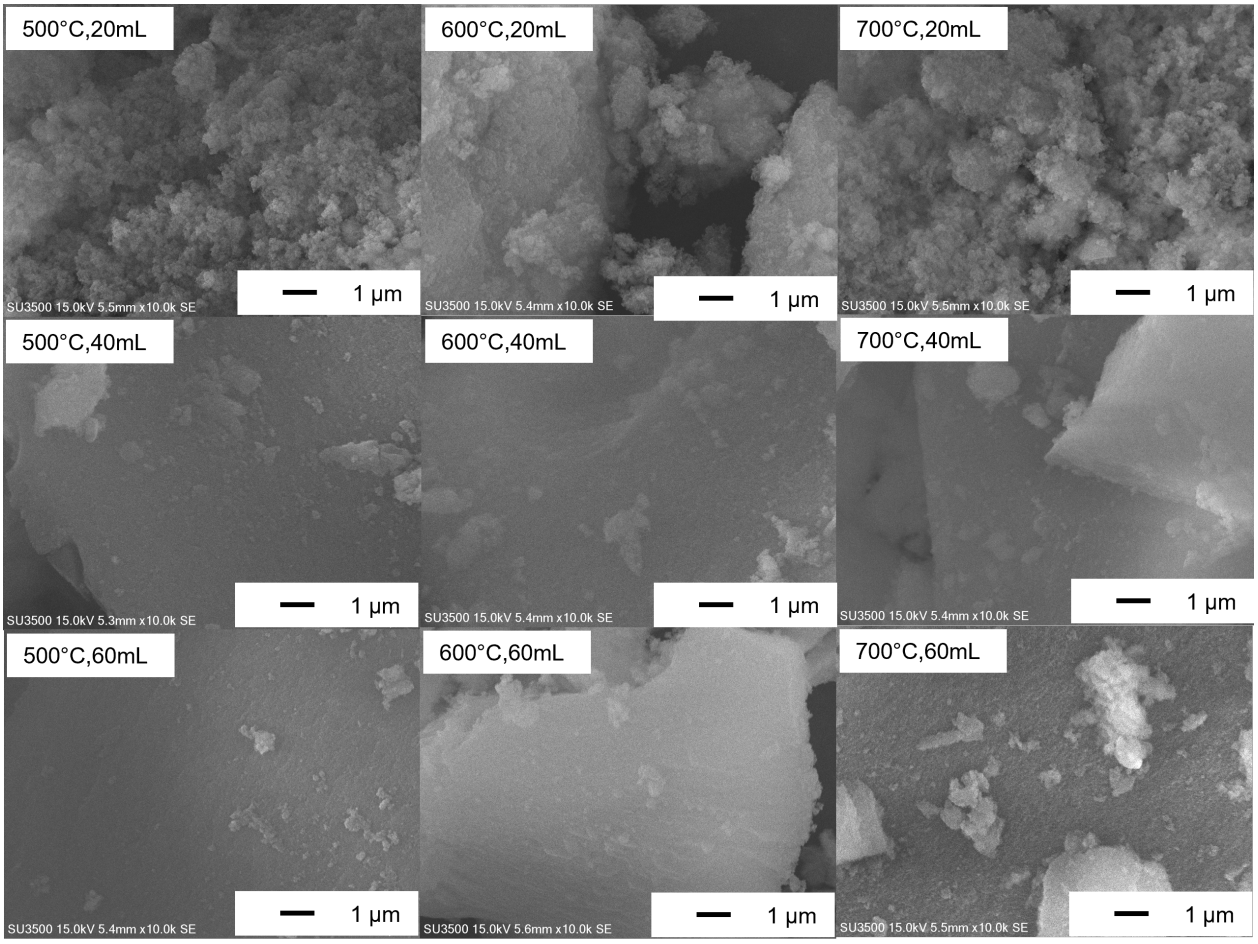

Figure 6. SEM images of silica nanoparticles synthesized at a 1:1.4 cullet to NaOH weight ratio under different fusion temperatures and water volumes (mL values indicate water volume used for dissolving 5 g fused material during sodium silicate solution preparation).

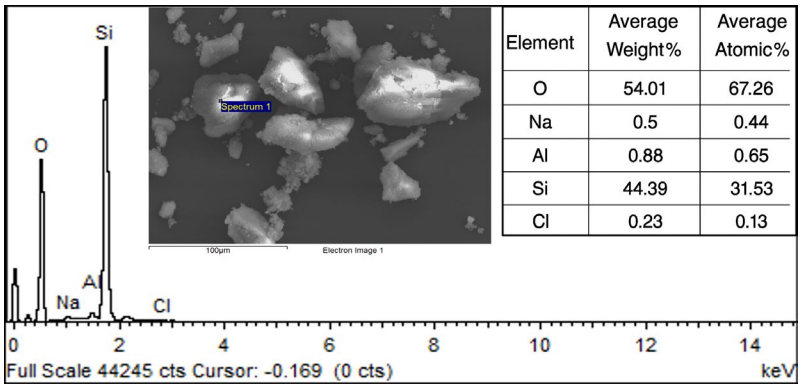

Element	Average Weight%	Average Atomic%
O	54.01	67.26
Na	0.5	0.44
Al	0.88	0.65
Si	44.39	31.53
Cl	0.23	0.13

Figure 7. EDX analysis of silica synthesized at a 1:1.4 cullet to NaOH weight ratio and fused at 500°C.

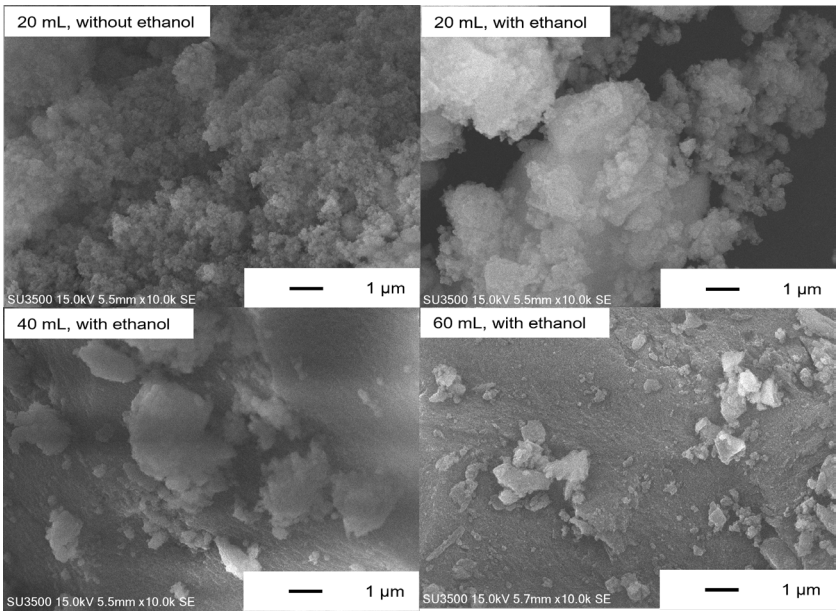

Figure 8. SEM images of silica nanoparticles synthesized with and without ethanol addition (mL values indicate water volume used for sodium silicate dissolution; ethanol added at 5 vol% during acid precipitation).

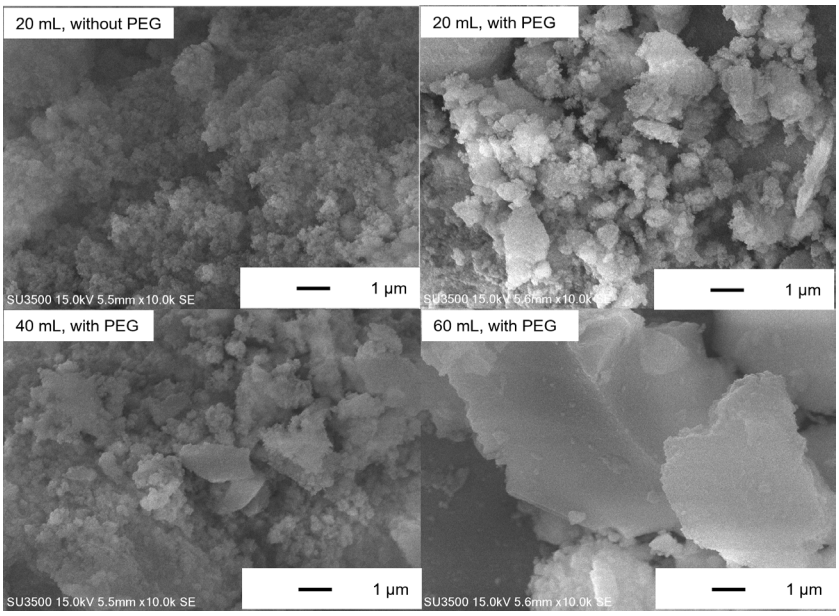

Figure 9. SEM images of silica nanoparticles synthesized with and without PEG 1000 addition (mL values indicate water volume used for sodium silicate dissolution; PEG 1000 added at 2.5 wt% during acid precipitation).

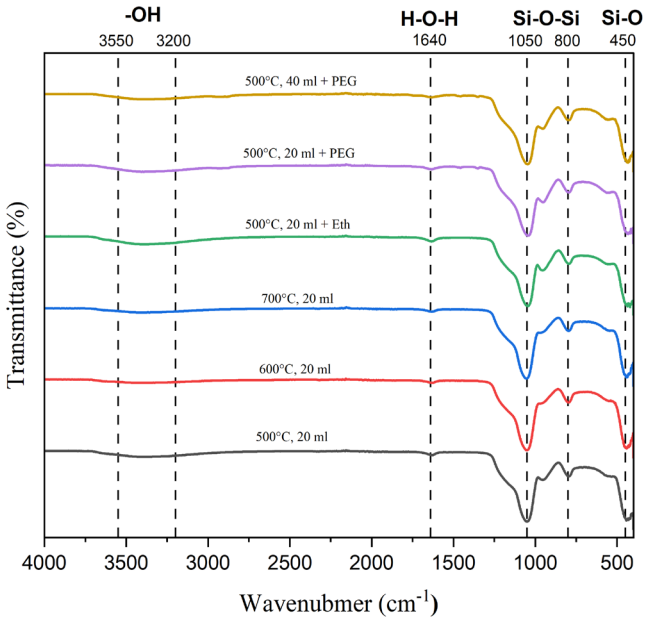

Figure 10. FTIR spectra of silica nanoparticles samples.

3.5 Effect of ethanol and PEG 1000 on particle morphology

To investigate the effects of additives on particle morphology and agglomeration, ethanol (5 vol%) and PEG 1000 (2.5 wt%) were introduced during the acid precipitation step. SEM images of silica nanoparticles samples prepared with and without these additives, focusing on samples synthesized at 500°C with a 1:1.4 cullet to NaOH ratio. The addition of ethanol (5 vol%) (Figure 8) did not show a significant reduction in agglomeration or particle size when the sodium silicate concentration varied. At 20 mL water volume, the effect remained inconclusive based solely on SEM images. For 40 mL and 60 mL water volumes, particles appeared similar in size and degree of agglomeration regardless of ethanol addition. Although ethanol is often reported to reduce agglomeration by lowering surface tension and altering hydrolysis condensation kinetics [34], in this study the effect was minimal. This limited influence may be due to the relatively low ethanol concentration (5 vol%), which was insufficient to significantly change the precipitation dynamics. Higher ethanol concentrations might induce more noticeable effects on particle size and morphology.

In contrast, the addition of PEG 1000 (2.5 wt%) (Figure 9) had a noticeable effect on particle morphology. It helped reduce agglomeration and particle size in samples prepared with 20 mL and 40 mL water volumes, where the sodium silicate concentration was lower. The surfactant effect of PEG 1000 likely prevented particle growth and agglomeration by adsorbing onto the particle surface and providing steric hindrance [35]. However, at 60 mL water volume (lowest sodium silicate concentration), particle size increased again despite the presence of PEG 1000, suggesting that the dilution effect dominated over the surfactant effect in this case.

3.6 FTIR analysis

The chemical structure of the synthesized silica nanoparticles was investigated using FTIR spectroscopy. Figure 10 shows the FTIR spectra of silica nanoparticle samples prepared under different conditions. All samples exhibited characteristic absorption bands of silica. The broad band observed at 3550 cm^{-1} to 3200 cm^{-1} was attributed to the O–H stretching vibrations of silanol groups (Si–OH) and adsorbed water molecules [36]. A distinct band around 1640 cm^{-1} was assigned to the H–O–H bending vibration of molecular water. The strong absorption near 1050 cm^{-1} corresponded to the asymmetric stretching vibration of Si–O–Si bonds, while the bands at approximately 800 cm^{-1} and 450 cm^{-1} were attributed to the symmetric stretching and bending vibrations of Si–O bonds, respectively [37]. These spectral features confirmed the successful synthesis of silica nanoparticles from solar panel glass cullet [38].

3.7 BET analysis

The specific surface area and pore characteristics of the synthesized silica nanoparticles were evaluated using BET analysis to understand the effect of PEG 1000 addition on the textural properties. The results, presented in Table 2, show that the sample with PEG 1000 exhibited a higher surface area of 372.34 $m^2 \cdot g^{-1}$ compared to 360.24 $m^2 \cdot g^{-1}$ for the sample without PEG. Both samples showed similar pore volumes 0.72 $cm^3 \cdot g^{-1}$ and 0.73 $cm^3 \cdot g^{-1}$, but showed notable differences in pore size distribution. The sample without PEG had a larger average pore size of 12.36 nm, while the sample with PEG showed a smaller average pore size of 8.91 nm. According to IUPAC classification, both samples contain primarily mesopores (2 nm to 50 nm), with PEG addition shifting the distribution toward smaller mesopores. The increase in surface area and reduction in average pore size observed with PEG 1000 addition are attributed to its surfactant role during precipitation. PEG absorbs onto particle surfaces, reducing agglomeration and limiting growth, thereby producing smaller, more dispersed particles with a denser mesoporous structure.

Reported surface areas of silica nanoparticles vary widely depending on synthesis methods and applications, ranging from 75 $m^2 \cdot g^{-1}$ for polymer composites and biomass-derived silica, to ~364 $m^2 \cdot g^{-1}$ for mesoporous silica used in dye adsorption [39–41]. The BET values obtained in this study are significantly higher than the 83.63 $m^2 \cdot g^{-1}$ previously reported for glass-derived silica [33]. These results confirm that the present synthesis route is highly effective, with PEG 1000 playing a key role in enhancing the surface area and improving the textural properties of the nanoparticles.

Table 2. BET analysis of silica nanoparticles synthesized with and without PEG 1000.

Sample	Surface area [$m^2 \cdot g^{-1}$]	Pore volume [$cm^3 \cdot g^{-1}$]	Pore size [nm]
Without PEG 1000	360.24	0.72	12.36
With PEG 1000	372.34	0.73	8.91

4. Conclusion

This study demonstrates an effective route for synthesizing high-purity silica nanoparticles from solar panel glass cullet, addressing both waste management and resource recovery. Optimized alkali fusion at a 1:1.4 cullet-to-NaOH ratio and 500°C achieved the highest yield while minimizing residue, while water volume was found to govern particle size through nucleation and growth dynamics. PEG 1000 addition further improved dispersion, reduced particle size, and enhanced surface area, whereas ethanol showed little effect. The resulting silica nanoparticles exhibited 95.12% purity and a surface area of 372.34 $m^2 \cdot g^{-1}$. These results highlight that combining process optimization with surfactant assistance enables the efficient production of high-quality silica nanoparticles from solar panel glass cullet, contributing to sustainable materials development.

Acknowledgements

The author gratefully acknowledges the Upcycled Materials from Industrial and Agricultural Wastes Research Unit (RU), Department of Materials Science, Faculty of Science, Chulalongkorn University, for financial support and research funding.

References

[1] REN21, "Renewables 2023 Global Status Report," *REN21 Secretariat*, 2023.

[2] IRENA, "Renewable Power Generation Costs in 2021," *International Renewable Energy Agency*, 2022.

[3] IEA, "Share of renewable electricity generation," *International Energy Agency*, 2024.

[4] D. C. Jordan, and S. R. Kurtz, "Photovoltaic degradation rates—an analytical review," *Progress in Photovoltaics: Research and Applications*, vol. 21, no. 1, pp. 12–29, 2013.

[5] S. Weckend, A. Wade, and G. Heath, "End-of-Life Management: Solar Photovoltaic Panels," *IRENA and IEA-PVPS*, 2016.

[6] V. Fiandra, L. Sannino, C. Andreozzi, and G. Graditi, "End-of-life of silicon PV panels: A sustainable materials recovery process," *Waste Management,* vol. 84, pp. 91–101, 2019.

[7] R. Deng, N. L. Chang, Z. Ouyang, and C. M. Chong, "A techno-economic review of silicon photovoltaic module recycling," *Renewable and Sustainable Energy Reviews,* vol. 109, pp. 532–550, 2019.

[8] C. E. L. Latunussa, F. Ardente, G. A. Blengini, and L. Mancini, "Life Cycle Assessment of an innovative recycling process for crystalline silicon photovoltaic panels," *Solar Energy Materials & Solar Cells,* vol. 156, pp. 101–111, 2016.

[9] J. K. Choi, and V. Fthenakis, "Crystalline silicon photovoltaic recycling planning: macro and micro perspectives," *Journal of Cleaner Production,* vol. 66, pp. 443–449, 2014.

[10] P. Dias, S. Javimczik, M. Benevit, and H. Veit, "Recycling WEEE: Extraction and concentration of silver from waste crystalline silicon photovoltaic modules," *Waste Management*, vol. 57, pp. 220–225, 2017.

[11] I. D'Adamo, M. Miliacca, and P. Rosa, "Economic feasibility for recycling of waste crystalline silicon photovoltaic modules," *International Journal of Photoenergy*, vol. 2017, Art. no. 4184676, pp. 1–6, 2017.

[12] M. M. Lunardi, J. P. Alvarez-Gaitan, J. I. Bilbao, and R. Corkish, "A review of recycling processes for photovoltaic modules," *Solar Panels and Photovoltaic Materials*, vol. 1, pp. 9–27, 2018.

[13] A. Theerapapvisetpong and S. Nilpairach, "Utilization of glass cutting sludge and sanitary ware sludge in ceramic pressed bodies," *Key Engineering Materials*, vol. 659, pp. 169–174, 2015.

[14] F. Matteucci, M. Dondi, and G. Guarini, "Effect of soda-lime glass on sintering and technological properties of porcelain stoneware tiles," *Ceramics International*, vol. 28, pp. 873–880, 2002.

[15] A. Tucci, L. Esposito, E. Rastelli, C. Palmonari, and E. Rambaldi, "Use of soda-lime scrap-glass as a fluxing agent in a porcelain stoneware tile mix," *Journal of the European Ceramic Society*, vol. 24, pp. 83–92, 2004.

[16] N. Marinoni, D. D'Alessio, V. Diella, A. Pavese, and F. Francescon, "Effects of soda-lime-silica waste glass on mullite formation kinetics and micro-structures development in vitreous ceramics," *Journal of Environmental Management*, vol. 124, pp. 100–107, 2013.

[17] M. Dondi, G. Guarini, M. Raimondo, and C. Zanelli, "Recycling PC and TV waste glass in clay bricks and roof tiles," *Waste Management*, vol. 29, pp. 1945–1951, 2009.

[18] V. Fiandra, L. Sannino, C. Andreozzi, and G. Graditi, "End-of-life of silicon PV panels: A sustainable materials recovery process," *Waste Management*, vol. 84, pp. 91–101, 2019.

[19] Y. Jiang, T. C. Ling, C. Shi, and S. Y. Pan, "Characteristics of steel slags and their use in cement and concrete—A review," *Resources, Conservation & Recycling,* vol. 136, pp. 187–197, 2018.

[20] M. Mirzahosseini, and K. A. Riding, "Effect of curing temperature and glass type on the pozzolanic reactivity of glass powder," *Cement and Concrete Research,* vol. 58, pp. 103–111, 2015.

[21] A. M. Rashad, "Recycled waste glass as fine aggregate replacement in cementitious materials based on Portland cement," *Construction and Building Materials,* vol. 72, pp. 340-357, 2014.

[22] Z. Chen, J. S. Li, and C. S. Poon, "Combined use of sewage sludge ash and recycled glass cullet for the production of concrete blocks," *Journal of Cleaner Production,* vol. 171, pp. 1447–1459, 2018.

[23] Y. Jani, and W. Hogland, "Waste glass in the production of cement and concrete—A review," *Journal of Environmental Chemical Engineering,* vol. 2, no. 3, pp. 1767–1775, 2014.

[24] A. Khmiri, B. Samet, and M. Chaabouni, "A cross mixture design to optimise the formulation of a ground waste glass blended cement," *Construction and Building Materials,* vol. 28, no. 1, pp. 680–686, 2012.

[25] J. X. Lu, and C. S. Poon, "Use of waste glass in alkali activated cement mortar," *Construction and Building Materials,* vol. 160, pp. 399–407, 2018.

[26] Y. Shao, T. Lefort, S. Moras, and D. Rodriguez, "Studies on concrete containing ground waste glass," *Cement and Concrete Research,* vol. 30, no. 1, pp. 91–100, 2000.

[27] W. A. A. Sudjarwo, and M. M. F. Bee, "Synthesis of silica gel from waste glass bottles and its application for the reduction of

free fatty acid (FFA) on waste cooking oil," *AIP conference proceedings,* vol. 1855, no. 1, p. 020019, 2017.

[28] Q. Guo, D. Huang, X. Kou, W. Cao, L. Li, L. Ge, and J. Li, "Synthesis of disperse amorphous SiO_2 nanoparticles via sol–gel process," *Ceramics International*, vol. 43, pp. 192–196, 2017.

[29] A. Akbari, R. Yegani, and B. Pourabbas, "Synthesis of poly (ethylene glycol) (PEG) grafted silica nanoparticles with a minimum adhesion of proteins via one-pot one-step method," *Colloids and Surfaces A: Physicochemical and Engineering Aspects*, vol. 484, pp. 206–215, 2015.

[30] S. Hussain, R. K. Singh, A. Kumar, S. S. Kumar, N. Kumar, G. Kumar, and A. K. Aman, "Natural silica nanoparticles from agricultural waste rice husk and its magnetic composites for its possible applications in semiconductor, catalytic activity and biomedical science," *Current Natural Sciences & Engineering,* vol. 2, no. 2, pp. 638–648, 2025.

[31] S. K. Natarajan, M. A. Sadiq, and M. A. M. Soudagar, "Utilization of waste glass powder in concrete," *Procedia Environmental Sciences*, vol. 35, pp. 579–588, 2016.

[32] F. Engström, D. Adolfsson, C. Samuelsson, Å. Sandström, and B. Björkman, "A study of the solubility of pure slag minerals," *Minerals Engineering*, vol. 41, pp. 46–52, 2013.

[33] Z. Asadi, and R. Norouzbeigi, "Synthesis of colloidal silica nanoparticles from waste glass powder as a low cost precursor," *Ceramics International,* vol. 44, no. 17, pp. 22692–22697, 2018

[34] I. A. Rahman, and V. Padavettan, "Synthesis of silica nanoparticles by sol-gel: size-dependent properties, surface modification, and applications in silica-polymer nanocomposites—A review," *Journal of Nanomaterials*, vol. 2012, p. 132424, pp. 1–15, 2012.

[35] Q. Guo, D. Huang, X. Kou, W. Cao, L. Li, L. Ge, and J. Li, "Synthesis of disperse amorphous SiO_2 nanoparticles via sol–gel process," *Ceramics International,* vol. 43, no. 1, pp. 192–196, 2017.

[36] R. Ellerbrock, M. Stein, and J. Schaller, "Comparing amorphous silica, short-range-ordered silicates and silicic acid species by FTIR," (in eng), *Scientific Reports*, vol. 12, no. 1, p. 11708, 2022.

[37] S. Saravanan, and R. S. Dubey, "Synthesis of SiO_2 nanoparticles by sol-gel method and their optical and structural properties," *Romanian Journal of Information Science and Technology*, vol. 23, pp. 105–112, 2020.

[38] S. K. Malpani, and D. Goyal, "Synthesis, analysis, and multi-faceted applications of solid wastes-derived silica nanoparticles: a comprehensive review (2010–2022)," *Environmental Science and Pollution Research*, vol. 30, no. 11, pp. 28321–28343, 2023.

[39] F. Bondioli, V. Cannillo, E. Fabbri, and M. Messori, "Epoxy-silica nanocomposites: Preparation, experimental characterization, and modeling," *Journal of Applied Polymer Science*, vol. 97, pp. 2382–2386, 2005.

[40] S. Liu, X. Chen, W. Ai, and C. Wei, "A new method to prepare mesoporous silica from coal gasification fine slag and its application in methylene blue adsorption," *Journal of Cleaner Production*, vol. 212, pp. 1062–1071, 2019.

[41] D. Kaliannan, S. Palaninaicker, V. Palanivel, M. A. Mahadeo, B. N. Ravindra, and S. Jae-Jin, "A novel approach to preparation of nano-adsorbent from agricultural wastes (Saccharum officinarum leaves) and its environmental application," *Environmental Science and Pollution Research*, vol. 26, no. 6, pp. 5305–5314, 2019.